

Retrospective Theses and Dissertations

1999

Design considerations and thermodynamic feasibility study of a meso-scale refrigerator

Nabil Shovon Ashraf
nsnabil2002@yahoo.com

 Part of the [Electrical and Computer Engineering Commons](#)
Find similar works at: <https://stars.library.ucf.edu/rtd>
University of Central Florida Libraries <http://library.ucf.edu>

This Masters Thesis (Open Access) is brought to you for free and open access by STARS. It has been accepted for inclusion in Retrospective Theses and Dissertations by an authorized administrator of STARS. For more information, please contact STARS@ucf.edu.

STARS Citation

Ashraf, Nabil Shovon, "Design considerations and thermodynamic feasibility study of a meso-scale refrigerator" (1999). *Retrospective Theses and Dissertations*. 2050.
<https://stars.library.ucf.edu/rtd/2050>

DESIGN CONSIDERATIONS AND THERMODYNAMIC
FEASIBILITY STUDY OF A MESO - SCALE
REFRIGERATOR

by

NABIL SHOYON ASHRAF

B. Tech. Indian Institute of Technology Kanpur, India, May 1997

A thesis submitted in partial fulfillment of the requirements
for the degree of Master of Science
in the Department of Electrical and Computer Engineering
in the College of Engineering
at the University of Central Florida
Orlando, Florida

Summer Term
1999

ABSTRACT

Recent advances in micro-fabrication technology have ushered a new era in miniaturization of chemical, environmental and energy systems. This foreseeable trend towards miniaturization in chemical, environmental and mechanical systems is expected to revolutionize the ways the human life is being perceived today. The high volume and mass reproducibility is seen as the striking aspect of micro-fabrication based miniature systems, offering economies far exceeding than the economies of scale obtained in large plants.

The focus of this thesis work is directed at the thermodynamic feasibility and preliminary prototype design for a meso-scale refrigerator. Miniaturization to sub-centimeter domain will enable configuring these refrigerator units as sheet architectures integrated in layers, facilitating efficient local control of temperature. In the design abstraction, the entire refrigeration unit, comprising motor-compressor, evaporator, condenser, valves and fluidic control, is to be fabricated from several layers of bonded silicon wafers. The material treated in this thesis provides a perspective on the actuation mechanism of the integrated rotor-compressor through an axial-drive high-throughput variable capacitance electrostatic disk motor and underlying stator assembly. The design optimization of the motor actuation dynamics to extract optimal set of design parameters is provided to yield reasonably good output power of the compressor.

Dedicated
to
my parents

ACKNOWLEDGEMENTS

I would like to express my sincere gratitude to my graduate Chair Dr. K. B. Sundaram and graduate Co-Chair Dr. L. C. Chow for their patient guidance, constant support and inspirational feedback towards completion of this research work. I wish to thank my committee members Dr. J. Kapat and Dr. I. Batarseh for their time, support and invaluable comments. I would also like to thank Dr. C. B. Gu for his initial contribution at the start-up of this research. Special gratitude is also due to my research group members and Mr. J. Vaidya, for their invaluable cooperation and support at every step of this research. Lastly, I wish to express gratitude to my beloved parents, who have always been an inspirational source to me to realize my goals.

TABLE OF CONTENTS

	LIST OF TABLES.....	viii
	LIST OF FIGURES.....	ix
1	INTRODUCTION.....	1
2	THE CONCEPT OF A MINIATURE REFRIGERATOR AND ITS THERMODYNAMIC FEASIBILITY.....	6
	2.1 REFRIGERATION PROCESS AND VAPOR COMPRESSION CYCLE.....	7
	2.1.1 VAPOR COMPRESSION CYCLE.....	8
3	STRUCTURAL UNITS AND DESIGN CONSIDERATIONS OF A MINIATURE REFRIGERATOR.....	12
	3.1 BUILDING MODULES OF THE PROPOSED REFRIGERATOR.....	13
	3.1.1 SELECTION OF SILICON AS A MECHANICAL MATERIAL.....	21

4	COMPRESSOR ACTUATION PRINCIPLE FOR ROTARY MOTOR DRIVE.....	24
4.1	PRINCIPLES OF SYNCHRONOUS ACTUATION FOR THE ROTOR COMPRESSOR.....	27
4.1.1	THEORETICAL DEVELOPMENT OF CAPACITANCE ACTUATION.....	27
4.1.2	DYNAMICS OF AXIAL DRIVE VARIABLE CAPACITANCE MOTOR.....	30
5	A NUMERICAL ANALYSIS OF STRUCTURAL PARAMETERS OF THE ACTUATION UNIT FOR OPTIMIZED POWER OUTPUT.....	35
5.1	THEORETICAL CALCULATION OF TORQUE AND POWER.....	37
5.2	OPTIMIZATION OF PARAMETERS FOR OPTIMUM POWER OUTPUT OF ROTOR-COMPRESSOR ACTUATION UNIT.....	43
6	AN OVERVIEW OF ELECTRO-QUASISTATIC INDUCTION MOTOR AND PERFORMANCE TRADE-OFF.....	49
6.1	INDUCTION MOTOR DRIVE PRINCIPLE AND PERFORMANCE CRITICAL PARAMETERS.....	51
7	CONCLUSION AND FUTURE WORK.....	55

Appendix.....59

A. Kinematical performance analysis of variable capacitance motor.....59

8 LIST OF REFERENCES.....63

LIST OF TABLES

1. Results of Parametric Analysis of the Actuation Unit.....48

LIST OF FIGURES

1. The Block-diagram of the functional units of a miniature refrigerator.....	9
2. Temperature-enthalpy diagram of a Vapor-compression system.....	11
3. Schematic cross-sectional view of the entire refrigerator's building modules.....	15
4. Compressor disk viewgraph with diffuser vanes and blades.....	16
5. Projected prototype structure of evaporator and condenser base unit.....	17
6. Projected coverplate of evaporator and condenser unit.....	17
7. Top view of stator and rotor disks employed in compressor actuation unit.....	18
8. Electric suspension circuit for axial drive motor levitation.....	21
9. Guiding force due to parallel plate overlap.....	29
10. Electrostatic variable-capacitance drive principle by spatial misalignment of rotor pads from stator.....	31
11. Electrostatic pulse drive waveform applied to stator pads.....	32
12. Rectangular pulse, capacitance and torque waveform.....	33

CHAPTER 1

INTRODUCTION

The ever-prevailing miniaturization of electronics has produced a far-reaching technological revolution and innovations experienced in modern era. In perfect accord with the ongoing developments in high-density electronics, engineers and scientists have acquired revolutionary success in definition of micro-technology-based MEMS systems, the micro-scale derivatives of conventional macro-scale electromechanical systems [1]. In a strikingly short period of time, micromechanics has evolved as a rich, diverse field that draws on multitudes of technical disciplines. Over the years, MEMS has recorded pronounced potential applications in medicine, consumer products, genetic engineering, aerospace and microsattellites, infra-red and RF communications, sensors for automobiles and chemical processing and microactuators in current and future tiny robotics and control [2-4].

The technology of microdynamics is based on the realm and functionalities encompassed by microelectronics but calls for distinctive and exemplary advances over it. The goal of a MEMS designer is to make fully assembled and well coordinated devices and system modules in a single silicon chip and supersede the incompetencies of conventional large-scale counterparts in realizing potential diversified applications.

The much-talked-about system-on-chip (SOC) design also benefits from MEMS field in the way, that this is one of the rare technology that ensures co-location of hybrid modules performing characteristic functions, for instance, sensing, computation, actuation, control, communication and power [5]. Systems with small dimensions have advantages in handling small parts with enhanced speed, accuracy and gentleness-sometimes beyond the limit of human manipulation and patience. Certain distinctive advantages that accrue from miniaturized devices are as follows:

(a) *Higher throughput*: The time for an operation scales with the system's linear dimension raised to roughly the first power, s^1 , which essentially implies that a system one-tenth the size of the original has the potential of performing task ten times faster!

(b) *Higher accuracy*: Much of the problems due to phenomena such as temperature coefficient of expansion, deflection and vibration becomes less troublesome as the size of the system decreases. This fact has led to the use of micro devices in accelerometers, pressure and temperature sensors, mass flow valves in fluidics and precision actuation of microrobots.

(c) *Gentleness and compactness*: The small forces and masses associated with small systems make them more gentle. On the other hand, the high-density integration suggests that a complete device can be built in light-weight smaller packages with decreasing manufacturing cost as compared to the massive mass and cost overhead entertained in conventional manufacturing of mechatronics. The above advantage also extends itself to the important consideration of cost of floor space in manufacturing plants.

Researchers now realize that the same economies of scale enjoyed in the mass production of microchips can apply to mechanical systems in leading newer design and development of MEMS structures and actuators. Since MEMS is defined by surface photolithography of silicon wafers, the overall system size is irrelevant and the relevant size metric is the minimum feature size. Based on this fact, a transition can be foreseen between micro and mesoscopic domain of the defined mechanical structures. One possible advantage of millimeter-sized mesoscopic actuators over microactuators is the driving force and power output of rotary disk motors, used as the constituents of the actuators. Therefore more electromechanical power conversion can be achieved in meso-domain at the expense of device size, which may be tolerable for certain applications. The driving factor behind this research work stems from the vision of a potential new device, a mesoscopically miniaturized refrigerator of the size of a few centimeters. The successful generation of this refrigerator can provide the much-wanted thermal management in electronic cooling applications of high-density chips and packages [6]. These lithographically-defined silicon refrigerator can be fabricated in high-number of batches to replace the traditional large sized fans used in cooling of microprocessors of computers and other electronic devices, providing the almost same order of power conversion required. Also the very nature of the distributed architecture of the different building modules of the refrigerating systems enables an inevitable transition from centralized cooling to distributed cooling processes that allow for the reduction of ducting system losses which are more pronounced for the presently exercised large-scale central heating and cooling equipment (heatpump/refrigerator) [3]. In essence, successful

development of miniature energy-conversion devices will radically change how energy is used in many sophisticated and important applications.

The successful development of micro-technology based refrigerator in layers of sheet as cooling modules can have profound impact on energy use in buildings. If configured, sheet refrigerators can be distributed throughout a building, eliminating the need for central cooling equipment. The largest obstacle arises from the invention and refinement of existing microactuators to power the integrated motor-compressor assembly of the proposed refrigerator. Much work have been done on devising microactuator-based devices employing electrostatic, electromagnetic and piezoelectric principles as well as thermopneumatic and shape memory alloy-driven diaphragm actuators [7-13]. From the applicability point of view, to function effectively within a vapor-compression-cycled mesoscopic refrigerator, as undertaken for the current research study, the compressor-actuation must be able to obtain a compression ratio in the neighborhood of 3:1 to maintain reasonable temperature lift between the evaporation and condenser chamber (12°C to 60°C). We propose efficient actuation through axial-drive high-throughput variable capacitance electrostatic disk motor (VCM) configured as both rotary stator and compressor-integrated disk rotor. The rotor is positioned on top of the stator with a few microns of gap existing between the two to provide the driving torque. The adopted actuation method supercedes the use of piezoelectric motors by providing higher driving torque through the strong electrostatic axial force coupling between compressor's rotor and underlying stator.

With the above viewpoint in the perspective, Chapter 2 describes the thermodynamic feasibility study of a miniature refrigeration unit. The building blocks of typical air conditioning system are recast to define analogous structural units of the proposed refrigerator.

Chapter 3 outlines and describes the required structural units and their design considerations.

Chapter 4 studies the compressor actuation principles for the rotor-integrated compressor drive. The concept of variable capacitance synchronous actuation will be discussed. Although, the major focus of this thesis is on synchronous actuation, certain advantages due to ease of lithographic fabrication and motor position control, suggest the asynchronous electro-quasistatic actuation principle to be pursued as a useful alternative to variable-capacitance drive actuation unit of the refrigerator.

Chapter 5 is designed to provide a numerical analysis of critical structural parameters of rotor-compressor and stator unit for extraction of optimized mechanical power. Optimization will be done for the case of VCM. Optimization parameters include: maximum overlap capacitance in the rotational plane, i.e. $C(\theta)$ in R- θ plane, number and size or pattern of the pads integrated on stator and rotor for efficient overlap or maximum overlap capacitance, minimum distance between adjacent pads or pitch length, rotor-stator separation for driving torque generation and the excitation pulse magnitude.

Chapter 6 will provide an overview of electro-quasistatic induction drive performance.

Chapter 7 draws the conclusion and suggests future work on this research from viewpoint of some involved challenges and their possible solutions.

CHAPTER 2

THE CONCEPT OF A MINIATURE REFRIGERATOR AND ITS THERMODYNAMIC FEASIBILITY

A refrigerator can be defined as a system that moves from a low-temperature reservoir to a high-temperature reservoir [14]. Through the proper use of regulatory control, these units may be used during all seasons of the year for various purposes. In the cooling season, the unit functions as a regular cooling unit and hence like a refrigerator. During the heating season, however, the refrigerant flow is reversed and it becomes a heating unit. Due to the widespread need and applications of refrigerators in maintaining a system temperature that is lower than the ambient temperature, the thrust of the research study is devoted to the thermodynamic study of the cooling cycles as well as miniature cooling modules serving the purpose of present-day refrigeration systems.

The next section is aimed at providing the vapor-compression cycle that provides a good coefficient-of-performance or (COP) metric and used as the principle building blocks to the miniature refrigerator module. A good knowledge of the vapor-compression cycle requires an intensive study of the individual process as well as the thermodynamic relationships that exist between these processes, applications and operating conditions but rather the choice relies upon particular requirements of the application [16]. Until recently, the fluid that most nearly met all the required qualifications of general-purpose

refrigerant was a fluorinated hydrocarbon of methane series, dichlorodifluoromethane (CCl_2F_2) under the trade name of refrigerant-12 (R-12). The recent advent of CFC-free/HCFC-free R134a liquid refrigerant makes it an ideal choice to be used in all macro and miniature air-conditioning systems, due to the added hazard-free reliable property [17]. In the design of miniature refrigerator, whose component architecture will be outscored in the next chapter, R134a is chosen as the operating fluid.

2.1 REFRIGERATION PROCESS

AND THE VAPOR COMPRESSION CYCLE

The refrigeration or cooling is a process of reducing and maintaining the temperature of the interior surrounding of a thermodynamic heat-flow system (i.e., refrigerator) below the temperature of external or ambient surroundings. The refrigeration system operates in a closed loop, constantly circulating the same working fluid or refrigerant from a high temperature reservoir to a corresponding low temperature one, indicating that the mass flow rate of the refrigerant is same at all points of the cycle. To limit the flow of heat into the refrigerated region to a specified temperature differential, it is necessary to isolate the region from its surroundings with a good heat-insulating material.

In any refrigerating process, the substance employed as heat absorber or cooling agent is denoted as refrigerant. The ability of liquids to absorb enormous quantity of heat as they vaporize is the basis of their selection in modern mechanical air-cooling or refrigeration systems. As refrigerants, vaporizing liquids offer a number of advantages over melting solids or pure gaseous refrigerants; that is, (1) the refrigerating effect can be

started and stopped at will, (2) the rate of cooling can be predetermined within small limits, (3) the vaporizing temperature of the liquid can be governed by controlling the pressure at which the liquid vaporizes and (4) the vapor can be readily collected and condensed back into the liquid state, so that the same liquid can be used regeneratively to provide a continuous supply of refrigerant in the operation of the cooling process [15]. There is no single refrigerant that is best suited for all different

2.1.1 VAPOR COMPRESSION CYCLE

Although there are several possible thermodynamic power cycles that can be used for the cooling process of the proposed refrigerator, the one that is widely recognized and employed is the vapor-compression cooling system. A typical vapor-compression system comprises of four basic units pictorially depicted in Figure 1:

- (1) An evaporator, whose function is to provide a heat transfer surface through which heat can be absorbed from the refrigerated space into the vaporizing refrigerant.
- (2) A vapor compressor, whose function is to remove the vapor from the evaporator, and to raise the temperature and pressure of the vapor to a point such that the vapor can be condensed with heat discharge to a normally available heat sink.
- (3) A condenser, providing a heat transfer surface through which heat passes from the hot refrigerant vapor to a heat sink reservoir.
- (4) An expansion valve, which throttles, reduces pressure as the refrigerant flows from high condenser pressure to the lower evaporator pressure.

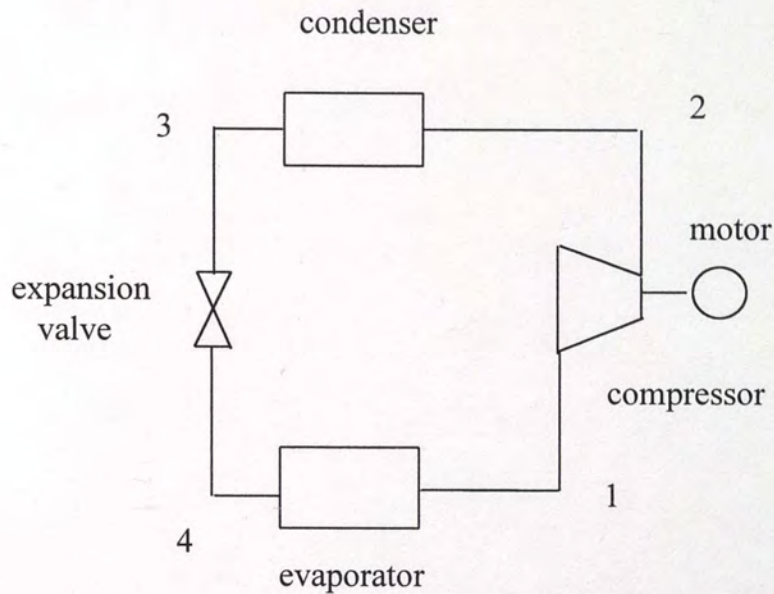


Figure 1: The Block-diagram of the functional units of a miniature refrigerator.

In addition to the above system units, several accessories are required for proper maintenance of the system: (5) a receiver tank, which provides storage for the condensed liquid so that a constant supply of liquid is available to the evaporator as needed; (6) a liquid flow line, which carries the liquid refrigerant from the receiver tank to the refrigerant flow control and (7) a refrigerant flow control, whose function is to meter the proper amount of refrigerant to the evaporator and to reduce the pressure of the liquid entering the evaporator, so that the liquid will vaporize in the evaporator at the desired low temperature.

The simple vapor-compression refrigeration cycle is made up of four fundamental processes in the order as follows: (1) expansion, (2) vaporization, (3) compression, and (4) condensation. The ideal cycle for vapor compression refrigerator is shown in Figure 2

as cycle 1-2-3-4-1. In process 1-2, saturated vapor at low pressure and temperature, enters the compressor, undergoes an constant-entropy adiabatic compression and emerges as a high-pressure and high-temperature superheated vapor. Work is done on the refrigerant vapor during the compression process by the actuation of the compressor, and the energy (enthalpy) of the vapor is increased by an amount exactly equal to the mechanical work done on the vapor. The energy equivalent of the work done during the compression process is referred to as *heat of compression* and is equal to the difference in enthalpy of the refrigerant at states 1 and 2. Before the superheated vapor can be condensed, the superheat must be removed and the temperature of the vapor lowered from the superheated state to the saturation temperature corresponding to its pressure. This task is accomplished in the process 2-3, where vapor is allowed to condense in the condenser after a rapid constant-pressure heat-removal step. Process 3-4 is a throttling type of adiabatic expansion in which the pressure of the liquid is reduced from the condensing pressure to the evaporator pressure, so that the enthalpy of the working fluid does not change during the process. This type of expansion occurs whenever a fluid is expanded through an orifice from a high pressure to a lower pressure, without incurring gain or loss of heat-content of the fluid, i.e., without any work done by the system. Finally, the cycle is completed in another constant-pressure(isobaric) and constant-temperature(isothermal) vaporizing process, in which the refrigerant is completely vaporized to saturation. The quantity of heat absorbed by the refrigerant in the evaporator is the difference between the enthalpy at the state 1 and 4, respectively [18].

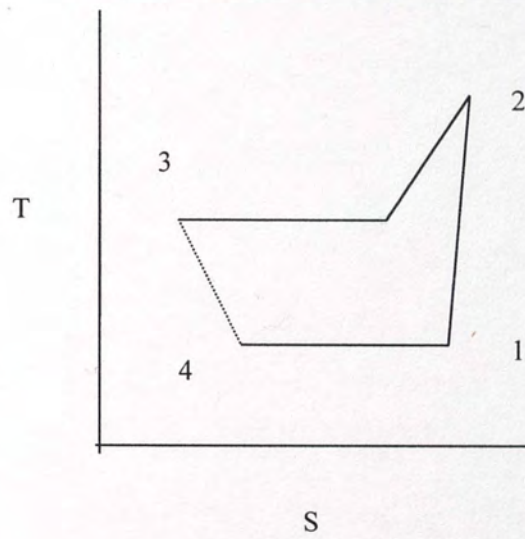


Figure 2: Temperature-entropy diagram of a Vapor-compression system.

Having delineating the essential building blocks of a refrigerator, the next chapter will discuss its miniature counterpart and how silicon serves as the material of choice.

CHAPTER 3

STRUCTURAL UNITS AND DESIGN CONSIDERATIONS OF A MINIATURE REFRIGERATOR

Evidences of exotic research and development programs on microtechnology-based applications are aplenty in the literature, which show great promise and profound impact on next generation energy and power-conversion devices. For instance, an extensive research is currently being conducted on developing the technology for micro-gas turbine generators capable of producing 50 watt of electric power in a package less than one cubic centimeter in volume [19-20]. Therefore, continued newer developments of miniature cooling systems and other potential propulsion and energy-efficient units, like the proposed meso-scale refrigerator, will bear a quantum leap in electric power sources, manifested by the potential to achieve more than ten times the power and energy densities of current batteries at competitive costs.

If we study the component structures of conventional air-cooling refrigeration systems, there is a growing optimism of co-fabrication of analogous miniature modules in pieces of integrated silicon wafers, with certain innovative reforms in the structural architecture [3,5]. If we achieve this target, the entire device will be manufactured in batches with a few cubic centimeter of volume. The concomitant advantage will be realization of kilowatt-level capacities from collection of arrayed layers or “sheet” architecture of refrigerators, assembled to facilitate miniature individual components to

sum their outputs favorably [3]. The presently conceptual scheme of assembling the sheet refrigerator in layers, with each layer containing arrays of microcomponents performing the typical one or the other cooling process steps, is worth pursuing. In such sheet refrigerators, one external layer may contain miniature heat exchangers, other microcompressors, the next microexpansion valves, and the last another external set of micro heat exchangers. In addition, there would undoubtedly be an internal layer that provides insulation to heat losses, which will degrade the temperature differential to be maintained between the evaporator and condenser units. The final product would resemble a large sheet with a series of coatings and a connection for electric-drive power and maintaining the capacity of the refrigerator. From an attainable target design capacity of 1 watt per square centimeter, integration of sheet refrigerators up to one square meter is capable of producing 10 kilowatt heating/cooling capacity, which is sufficient to heat and cool an average house besides being useful for electronic cooling of large embedded microprocessors, used for personal and mainframe computers.

3.1 BUILDING MODULES OF THE PROPOSED REFRIGERATOR

Thermal energy-conversion devices systems encompass multitudes of technical disciplines and design aspects. The architecture of the overall device is influenced by thermodynamics, while the design of system's components is determined by fluid and structural mechanics and system performance by electric and fabrication concerns. Figure 3 shows a cross-sectional view of the prototype refrigerator in its entirety. For the projected high-performance miniature refrigerator, the following structural components are envisioned:

(1) Integrated actuation unit: This unit, in essence, accomplishes the compression process of the previously described vapor-compression refrigeration system by actuation of the compressor to generate power in response to work done on the liquid refrigerant. The entire unit can be fabricated photolithographically on the silicon surface with a piece of silicon disk stator and separately forming two pieces of disk rotor and compressor, respectively and successive bonding of the two pieces, giving rise to one robust integrated motor-compressor. The actuation unit is oriented in such a way that rotor-compressor is axially positioned atop the stator. Both the stator and rotor disk have an inner hole, used for support of a central hub bushing and allows frictionless rotation. For variable capacitance synchronous actuation, a certain number of thin film pads are deposited extending in various shapes from the center to the periphery of the stator. A different set of pads are also deposited on the rotor back surface in a way such that, rotation takes place by maximum overlap capacitance-generated torque and force components. The compression process is attained by the wedge-shaped diffuser vanes having a much larger inner orifice cross-section, thermodynamically determined with respect to outlet orifice cross-section. These vanes are configured in large number on the surface of compressor and enable transition from a low temperature and low pressure state to a high temperature and high-pressure state as the compressor revolves at significantly high rpm, providing an overall centrifugal action on the vapor refrigerant that flows through it from stator to rotor-compressor.

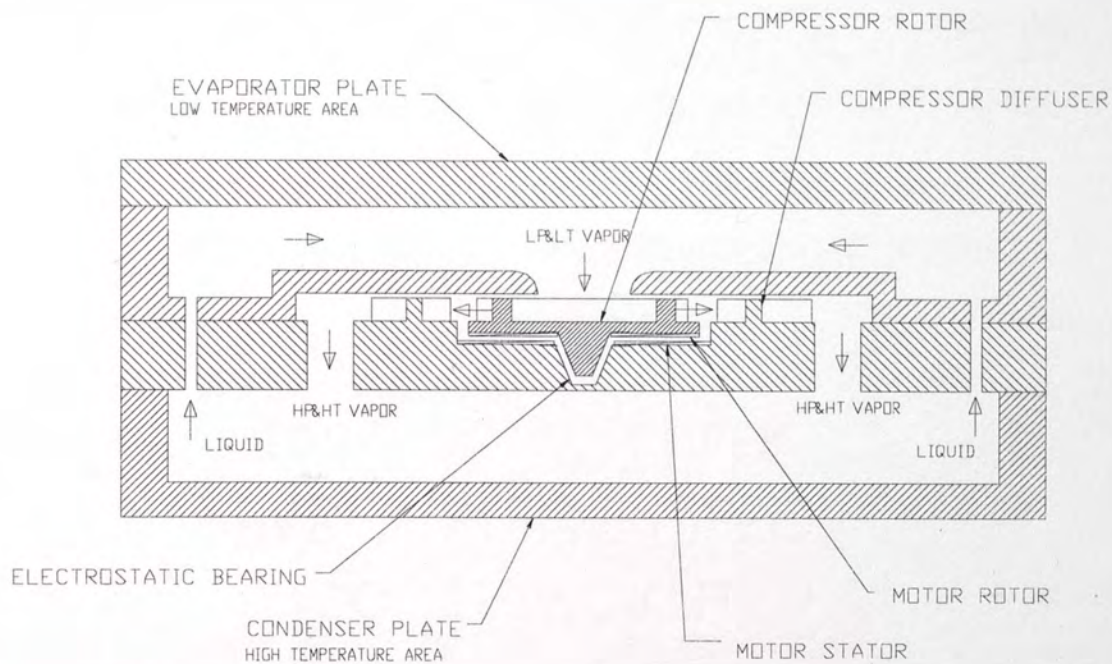


Figure 3: Schematic cross-sectional view of the entire refrigerator's building modules.

(2) Miniature evaporator and condenser plate: One possible design strategy of miniature heat-exchangers as evaporators and condensers is forming grooved microchannels or layers of tightly packed fins in silicon wafers. Since, heat flux to or from a channel is largely a function of the surface area-to-volume ratio, conduction along the surface of the serpentine fins enables efficient and rapid heat transfer than their large-sized counterparts. Microchannel-integrated heat sinks have already been demonstrated in tests using one-phase flow to provide high cooling capacities [3]. Heat transfer rates in the area of 100 watts per square centimeter (with a temperature difference of 15° to 20°C) have been experimentally verified. Unfortunately, frictional effects within a

microchannel fin heat exchanger also routinely scales with the inverse of diameter. For this reason, the most intriguing issue for miniscule condensers and evaporators is the pressure drop, or the pumping power required to overcome pressure drop through the heat exchanger. It has been demonstrated as an example in [3] that considering for a particular liquid refrigerant (choosing R-124), if we assume heat transfer results in only change of enthalpy for the vaporized refrigerant, the heat of vaporization(ΔH_v) that is absorbed or released upon evaporation or condensation is observed to be 150 joules per gram or in rate of 150 watts/g/sec. That is to say, for every gram per second of coolant condensing or vaporizing through the heat exchanger, approximately 150 watts of energy transfer are attained. Inverting this ratio clearly establishes the fact that within a miniature evaporator or condenser, refrigerant flow of 0.007 gram per second is needed to provide one watt of heating or cooling; suggesting that since flow rate is minimal, low pressure drops are feasible. Figure 4 shows one possible schematic of compressor unit.

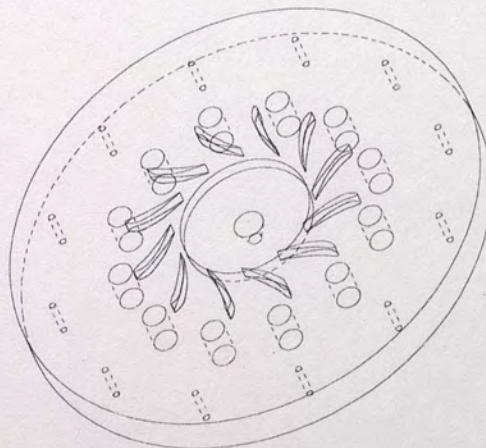


Figure 4: Compressor disk viewgraph with diffuser vanes and blades.

Figure 5 & 6 show the evaporator base plate configuration and the base cover, respectively. The stator and rotor disk diagram is shown in Figure 7 next. The separation between the stator and rotor-compressor is about 5 microns and large actuation torque can be generated to achieve compressor rpm as high as 3×10^5 . The disk rotor and stator both have an overall outer diameter of 12 mm and thickness of 0.6mm. The inner central hub for axial positioning, has a diameter of 2 mm.

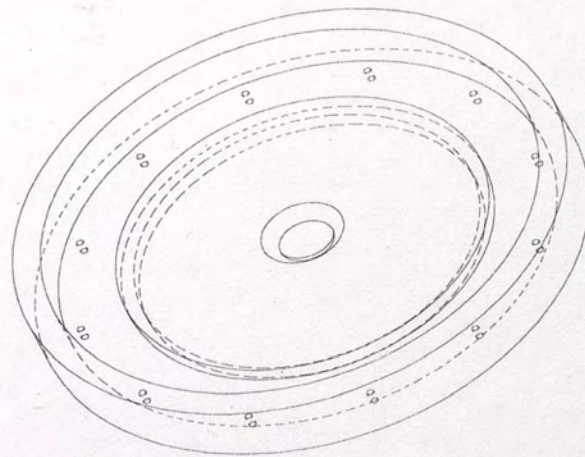


Figure 5: Projected prototype structure of evaporator and condenser base unit.

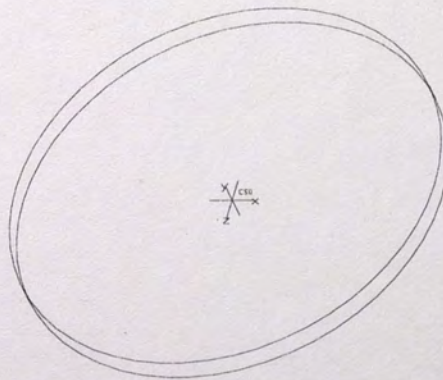
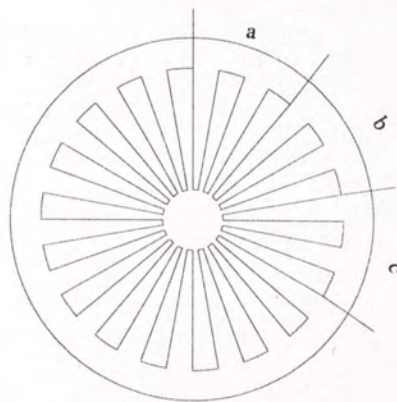
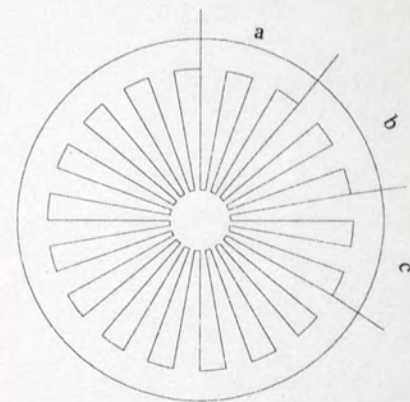


Figure 6: Projected cover plate of evaporator and condenser unit.



Electrostatic Stator



Electrostatic Rotor

Figure 7: Top view of stator and rotor disks employed in compressor actuation unit. The actual number of stator pads will differ from that of rotor.

(3) The in-situ fabrication of actuation and control IC: Since the synchronous excitation of rotor-compressor requires modulation of charge overlap between rotor and stator pads in a temporal fashion, the stator pads need to be provided with periodic alternating voltage (sinusoidal, square wave, etc.). It has been observed in various test procedures that for a unipolar square wave pulse, where the amplitude level switches from maximum value to ground, the rotor revolves in both clockwise and anticlockwise directions equally well and maximum torque and power conversion efficiency can be obtained. Since the actuation mode is entirely digitized, the recent developments in high voltage CMOS circuits auger well for the fabrication of IC-processed stator drive circuit without additional fabrication complexity. Several approaches have been hinted in literature to

fabricate high voltage devices in the vicinity of 150 volts with CMOS circuitry. The typical switching power MOSFETs, used in power converters and inverter-fed motor drive and control in current industry applications, can be integrated on-chip in multiple stages of voltage amplifying circuitry to generate the required pulse voltage level and duty-cycle(variation in pulse on-off width). Recently, an on chip single-stage CMOS amplifier, using PMOSFET cascode devices, have been fabricated to provide an 85 volt output swing. The design and topology of IC control circuit for more higher voltage generation warrants thorough research and investigation and is underway for our current research work. Also, the interconnection of the IC network to the stator pads in a well-orchestrated manner such that proper synchronism is obtained, poses considerable challenges and will need multilevel routing with dielectric isolation between each connective layer. These are the design studies that will be the subject for future work.

(4) Levitation circuitry for upholding the rotor separated from stator in thin space:

Although this IC unit is not a part of the actual vapor-compression system of the proposed refrigerator, this is an integral unit to be realized in order to provide rotational equilibrium of the high rpm compressor, rotor-positional alignment and stability [21-23]. On the other hand, all types of electrostatic motors suffer from wear and tear introduced by contact and bearing friction. Frictional forces in these devices are a result of mechanical contact between moving and stationary surfaces, and are compounded by the generation of large electric field in the micro-gap between moving rotor and stationary stator. Moreover, the extremely small dimensions of micromotors prohibit the use of conventional bearings. Hence, for high compression ratio of the compressor aided by

high rpm, elimination of mechanical contact between moving and stationary parts will be desirable. This could be alternatively achieved by implementing a closed loop control of the rotor, but the design issues are more intensive in comparison to a levitation mechanism that would keep the rotor aligned to the stator by providing precision-directional attractive/repulsive forces, subsequently compensating for the rigorous position-control loop design. Also, since the rotor is lifted by levitation force, contact friction losses can be eliminated. Two types of suspension method have drawn attraction among the engineers and researchers: (1) electric suspension, (2) magnetic suspension [9,24]. For application and performance, electric suspension method is the most feasible design that can be incorporated efficiently into the actuation unit. For simplicity, only the suspension principle will be outlined here.

Levitation mechanisms using up to three independent resonant circuits have been cited in the literature [25]. The designs utilize a resonant circuit with the conducting pads on the stator as its capacitor and a small external inductor and is driven by a high frequency alternating current. In the designs chosen by the authors, the revolving rotor lies under the stationary rotor. Hence the electrostatic attraction force between the corresponding pads on the stator and rotor provides the balancing suspension force to hold the rotor weight. By appropriately tuning the L-C circuit parameters to supply frequency, rotor is shown to positioned freely suspended in the microgap. In the design of this levitation circuit [25], electrostatic attraction principle was used, as shown in figure 8. But, for the proposed structural unit orientation and design of the refrigerator, the stator lies under the rotor-compressor and hence a vertical upward thrust is necessary to

pull the rotor up against its weight. Design in this particular arena is still in its infancy and requires further manipulation and assessment.

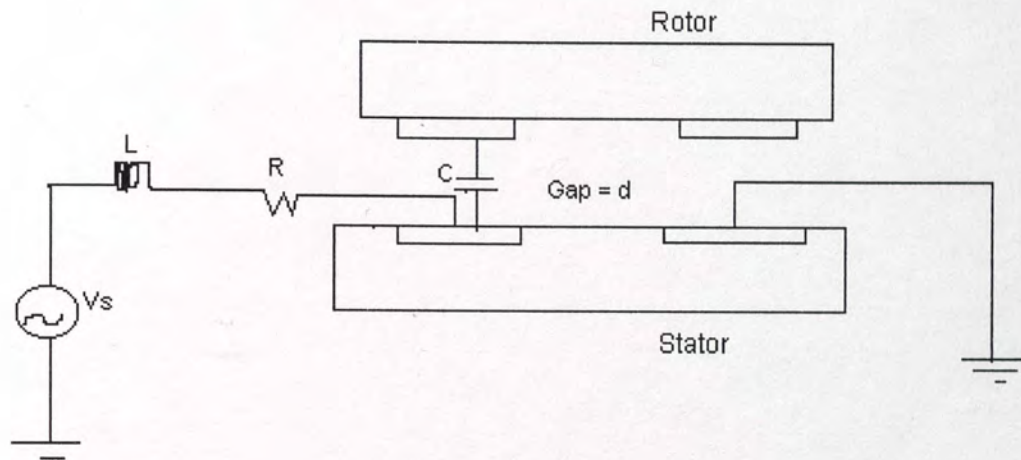


Figure 8: Electric suspension circuit for axial-drive motor levitation.

(Stator and rotor positions are interchangeable. For stability oscillation frequency of LC tuning circuit should be less than supply frequency.)

3.1.1 SELECTION OF SILICON AS A MECHANICAL MATERIAL

It is a point of little doubt that, in the same way that silicon has already revolutionized the modern era of infinitesimal electronics, this versatile material is all set to alter the conventional perceptions of miniature mechanical devices and components—drawing an increasing number of researchers to pursue single-crystal silicon wafers as their material of choice. The basis of choice for silicon for highly compact power and aerodynamic devices is risen due to its already well-established advanced micro and nano-fabrication technology, which can be used taking advantage of its high-precision

and high-strength mechanical property, to build miniaturized devices and components interfaced with control electronics and integrated in a single chip. Four factors have played crucial roles in this phenomenal success: (1) silicon is abundant and the typical industry-manufactured wafer is cost-effective. In addition, it may be the only material, in contention with silicon carbide and other ceramic material, which can be controllably processed to unparalleled standards of purity and perfection. (2) Silicon processing involves deposition of thin film layers which are highly amenable to miniaturization. (3) Ease of definition and reproduction of various etched and released device shapes and patterns in silicon using planar photolithography and SiO_2 etching by deep anisotropic etching techniques. The development of successful etching techniques to produce grooved and other structures is yet to be accomplished for certain ceramic and highly promising silicon carbide material. In silicon, established microfabrication process has been able to generate very high aspect ratio (depth/width) suspended structures in all forms of configuration with a few mask patterns and process sequence complexity. (4) The ultimate driving factor to silicon wafers is its batch manufacturability. The unit of production for VLSI ICs, i.e. the wafer contains millions of identical chips. This high-density integration certainly paved the way to produce similar chips of miniature consumer devices in a single wafer for all ranges of commercial consumer products.

While silicon has the seemingly singular potentiality for present and future generation MEMS and power-engines, the relatively high thermal conductivity of silicon in room temperature, makes its application limited in certain heat-transfer application, such as refrigerators, turbines and power generators etc. Due to susceptibility to breakdown and failure of high-actuation moving parts built in silicon, silicon carbide

microactuators have been studied and constructed [26]. In a more recent survey, it has been shown that thermoelectric devices could be a viable option [27]. Efficiency and materials are major factors affecting the performance of thermoelectric microdevices. The efficiency of thermoelectric devices depend on the non-dimensional factor ZT , which is defined as $ZT = S^2 \sigma T / k$, where S is the Seebeck coefficient, σ is the electrical conductivity, T is the absolute temperature and k is the thermal conductivity. A higher value of ZT increases the efficiency of thermoelectric devices. If ZT can be increased to 5-6, they will approach Carnot efficiency, making them more efficient for power engines and cooling refrigerators. But, how such thermoelectric device turns amenable to deep-level micro-photolithography and sacrificial etching processes without degrading surface texture, will be the issue the designers need to confront with.

CHAPTER 4

COMPRESSOR ACTUATION PRINCIPLE FOR ROTARY MOTOR DRIVE

As can be seen from the vapor-compression refrigeration system, the design of miniature compressor constitutes the largest technical challenge in developing the proposed miniature refrigerator system. The compressor rpm and refrigerant flow rate are critical to compressor capacity in the sense that compressor will displace in any given interval of time, the same mass of vapor as that generated in the evaporator in that same time interval. The refrigeration system's cycle efficiency is governed by a parameter known as coefficient of performance (c.o.p.) and is stated as the ratio of the heat absorbed in the refrigerated space to the heat energy equivalent of the energy supplied to the compressor, that is,

$$\text{Coefficient of performance} = \frac{\text{Heat absorbed from the refrigerated space}}{\text{Equivalent heat energy to the compressor}}$$

For the chosen refrigerant (R-134a) and the evaporating liquid and condensing vapor temperature of 12°C and 60°C, respectively, the thermodynamic enthalpy values for the four different states in the vapor compression cycle provides a c.o.p. of 3.28 with

compressor isentropic efficiency of 0.78. The specific work requirement for the compressor also suggests a considerable increase in compressor rpm to give rise to such work conversion efficiency. In essence, for the heat-pump to function properly, the meso-scale compressor must be able to push hard. The early-generation of work of 90's has been occupied with successful realization of such high-efficiency and high-speed microactuators. Over the years, considerable research was devoted to electrostatic versus electromagnetic actuation mechanism, shape-memory alloy actuation of microrobots and linear actuators, thermally-driven phase-change actuators, piezoelectric ultrasonic actuation with no bearing friction, etc. It turns out that, each particular actuation mechanism suits a predetermined application and the trade-off between actuation mechanisms will determine the ultimate choice of actuator for a selected performance level. It can be quite clearly seen that, the rotor-compressor designed for the actuation module of the proposed refrigerator is a high-rpm rotating device and hence requires high driving torque. The clustered family of shape-memory-alloy, thermally driven phase-change and piezoelectric ultrasonic actuators will not be able to impart the sizeable torque required to keep the rotor in its rotary trajectory, since they can only be used to generate series of linear miniscule movements in the sensory and actuation systems. Recently, thermopneumatic microactuators have been built and tested to be capable of producing reasonable compression action. But, their application in miniature heat engines received a setback owing to low efficiencies at the required rpm and operating power level of the compressor. Therefore, the only candidate that can be successfully employed is the electrostatic or electromagnetic drive, which underlies the operation of all present-day large electric motors.

In assessing the performance of miniaturized motors, the power per unit volume and efficiency are the two most important criteria. In the case of the traditional electromagnetic motor with its modern variant, both the power per unit volume and the efficiency are reduced when the same design is implemented in a scaled-down version. The reason is attributable to the fact that the energy dissipation in the magnetic coils relative to the electric power consumed becomes greater with increasing miniaturization of motor geometry. The operation of the electrostatic motor is based on the forces which electric fields exert on electric charges. It contains no coils, and the dissipation is very low, owing to charge transport in an arrangement of short electrodes of metallic thin films connected in parallel, and to dielectric losses. Therefore high electromechanical power conversion compares favorably for electrostatic motor with that of an electromagnetic motor of the same size. The other thrust for electrostatic drive emerges from high-density silicon VLSI compatibility, enabling us to fabricate different sizes and shapes of electrode patterns and good insulation films with consummate ease. Sub-cm (meso domain) electrostatic drive is facilitated by additional contribution from the following factors: (1) Thin insulation layers withstand higher electric field than thick layers. Thin insulation films of high quality are readily obtained by state-of-the-art silicon processes. (2) The electrostatic force is generated by charge overlap or surface film interaction and obeys a favorable scaling law in small dimension. Furthermore it needs only two thin electrodes separated by an insulation layer to form a high-strength electric field confined between the electrodes. On the other hand, electromagnetic force is the body force and needs considerable "ampere turns" to produce enough magnetic field,

which poses good fabrication complexity. Based on this observation, the electrostatic actuation mechanism is pursued for the design of the compressor. Since an electrostatic actuation involves both synchronous and asynchronous excitation, another performance-level trade-off is needed to arrive at one singular solution. For the current work, the synchronous actuation is obtained by variable-capacitance rotary drive principle or VCM method and will be discussed hereafter. The alternative method of electroquasistatic drive principle employing asynchronous excitation will be treated in Chapter 6, during which a brief overview of actuation mechanism of asynchronous motor will be discussed. In the course of the discussion, the relative advantages of asynchronous drive over synchronous will be enumerated for an ultimate design and performance trade-off.

4.1 PRINCIPLES OF SYNCHRONOUS ACTUATION EMPLOYED FOR THE ROTOR-COMPRESSOR

The planar photolithographic micron and sub-micron fabrication process in silicon has realized the feasibility of devising a high-performance electrostatic synchronous motor by the variable overlap of the conducting plates on the rotor and stator, giving rise to variable capacitance with rotor and stator position. The theoretical development variable-capacitance driven torque and force is discussed below before venturing into the detailed excitation dynamics.

4.1.1 THEORETICAL DEVELOPMENT OF CAPACITANCE

ACTUATION

From electrostatics, it is well known that two conducting parallel plates separated by an insulating layer create a capacitor with the capacitance given by,

$$C = \epsilon_r \epsilon_0 w \frac{l}{d} \quad (4.1)$$

where w is the width of the plates, l is the length of plates, d is the separation between the two plates and ϵ_0 and ϵ_r are the free space and relative permittivities. Now if a voltage is applied across the two plates, the potential energy of the capacitor is [28]

$$U = -\frac{1}{2} CV^2 = -\frac{\epsilon_r \epsilon_0 w l V^2}{2d} \quad (4.2)$$

The minus sign is indicative of the energy lost by the voltage source. The force exerted in any of the three directions (w , l , d) is given by the negative partial derivative of the potential energy in each of the three directions. For a hypothetical calculation of force, for example, in the w direction, an overlap of amount x is considered across the two plates as shown in the following Figure . In terms of the overlap x , the potential energy stored in the capacitor is modified to,

$$U = -\frac{\epsilon_r \epsilon_0 x l V^2}{2d} \quad (4.3)$$

and taking the derivative with respect to x , gives the force in the w direction as,

$$F_w = -\frac{\partial U}{\partial x} = \frac{1}{2} \frac{\epsilon_r \epsilon_0 l V^2}{d} \quad (4.4)$$

The forces in the l (along the length) and d (along the separation) can be similarly calculated and are omitted for brevity. As one plate is moved in terms of varying overlap parameter x , the potential energy stored in the overlapping parallel plate region changes, while the fringing areas remain nearly constant. The fringing effects at the edges of the plates are very difficult to calculate, and it is fortunate that they do not change significantly with respect to central-area field as the plates move and create substantial overlap, reducing computational complexity. The nature of force expressed in equation (4.4) suggests that when two plates of thin separation are slightly displaced spatially with respect to each other, a force parallel or tangential to the surface of the plates is developed, which subsequently tends to realign the plates. It is this aligning force which is the basis and driving factor behind rotary drive electrostatic motors. Also equation (4.4) shows that the aligning force is proportional F_w to the length of the edge l . Therefore, force per unit edge, f_w (which is independent of length of the thin film pads), is a useful parameter and is given by,

$$f_w = F_w / l = \frac{1}{2} \frac{\epsilon_r \epsilon_0 V^2}{d} = \frac{1}{2} \epsilon_r \epsilon_0 d E^2 \quad (4.5)$$

The Figure 9 shows how this force is formed between the parallel plate capacitor.

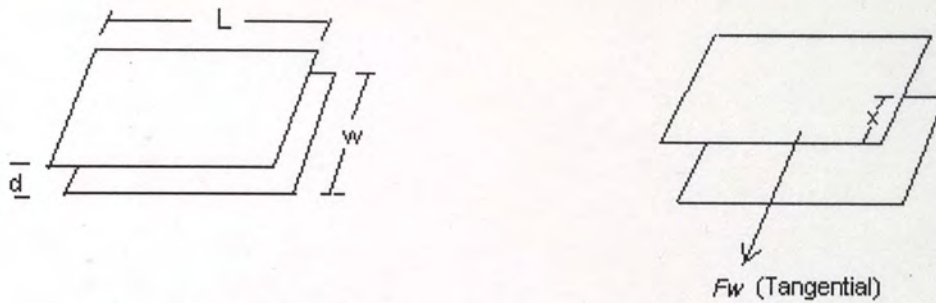


Figure 9: Guiding force due to parallel plate overlap.

The force depends on electric field squared, $E = V/d$, hence the key to high actuation drive is maximizing the E field, which can be achieved more effectively by decreasing the separation between the two parallel plates without violating the insulation failure or breakdown strength of the dielectric.

4.1.2 DYNAMICS OF AXIAL DRIVE

VARIABLE CAPACITANCE MOTOR

The inherent dynamics of rotary-drive axial variable capacitance motor can be explained by applying the principle developed conveniently for linear-drive motor [28]. Since for a particular snapshot and short-range of spatial arrangement, the rotor and stator poles can be treated as parallel plate poles (neglecting regions of pole curvature at the edges) and are axially positioned with respect to each other (rotor and stator is centrosymmetric and rotor is atop the stator). A simple cross-sectional schematic of front-view will look like the Figure 10, with pole position pairs denoted by A-A', B-B' and so on.

When a voltage is applied to one of the misaligned plates, i.e., on the stator plate (designated by A'), a force as calculated in the previous sub-section moves the rotor to a

small displacement in such a way that the pads A-A' are aligned leaving an overlap or misalignment in B-B', as shown in the Figure 10. From this characteristics, it is evident that when the rotor is at rest, all the pads on the rotor is aligned with corresponding pads on the stator, which is also known as equilibrium state. For the initiatory torque or force on the stator, which is also known as equilibrium state. For the initiatory torque or force on the rotor to be developed, since one of the rotor pad position needs to be displaced with respect to the corresponding pole location on the stator when the stator voltage is applied, the number of pads on the rotor will be essentially different from that on the stator to sustain the rotational movement. The judicious choice of the precise number of pads both on the stator and rotor is a design issue and will be revisited in Chapter 5 for

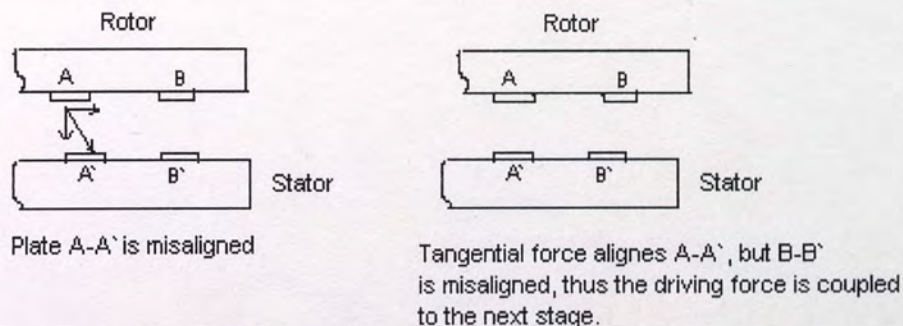


Figure 10: Electrostatic variable-capacitance drive principle by spatial misalignment of rotor pads from those of stator.

optimum torque and power generation. Now as plates B-B' are misaligned, another restoring force causes a motion in the rotor and tries to maintain the equilibrium state that leads to unidirectional movement throughout the excitation sequence. Since all other pads including B-B' in the vicinity of A-A' are also misaligned when A-A' position is aligned, the actual driving force which will rotate the rotor in a singular direction (clockwise or anticlockwise) will be determined by the strength or magnitude of the force as developed

by overlap area of the parallel plates, respectively. By differentially “phasing” the conductive and non-conductive portions of the top and bottom plates of the different capacitors in a perfect spatio-temporal fashion, a resultant singular motion can be generated in either direction for every instant during which a pulse is applied. For balanced and synchronous excitation, the required voltage waveforms are constituted by three-phase alternating excitation pulse voltage. During one full period of the applied one-off pulse train, the rotor turns half of its revolution. If we relate the voltage pulse, as shown in the following Figure 11, with respect to rotor revolution, in the quarter revolution when the misaligned rotor and stator blades are approaching each other, there is a voltage between them due to the presence of pulse during this interval and an attractive force is generated between the plates.

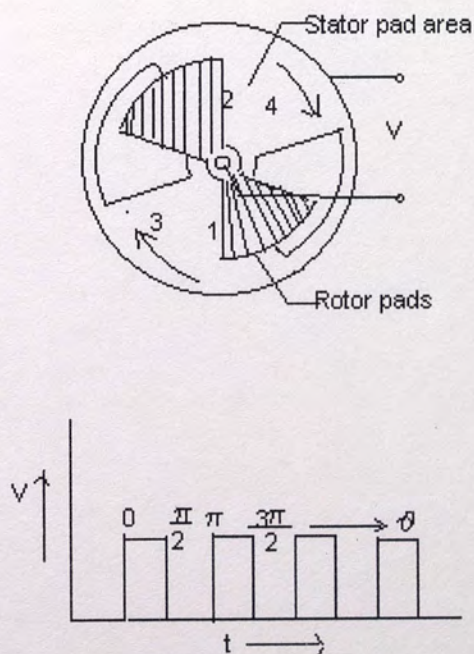


Figure 11: Electrostatic pulse drive waveform applied to stator pads.

During the next quarter revolution of the rotor, no pulse exists and the rotor continues to rotate by its own inertia. Although the torque in one period shows marked fluctuation, the motion is synchronous with the period of the pulse train, i.e., supply frequency, in the sense that it rotates in step with the supply voltage.

For the particular VCM actuation, a square wave pulse is chosen and the variation of capacitance with time as shown in the following Figure 12, assumes a triangular shape.

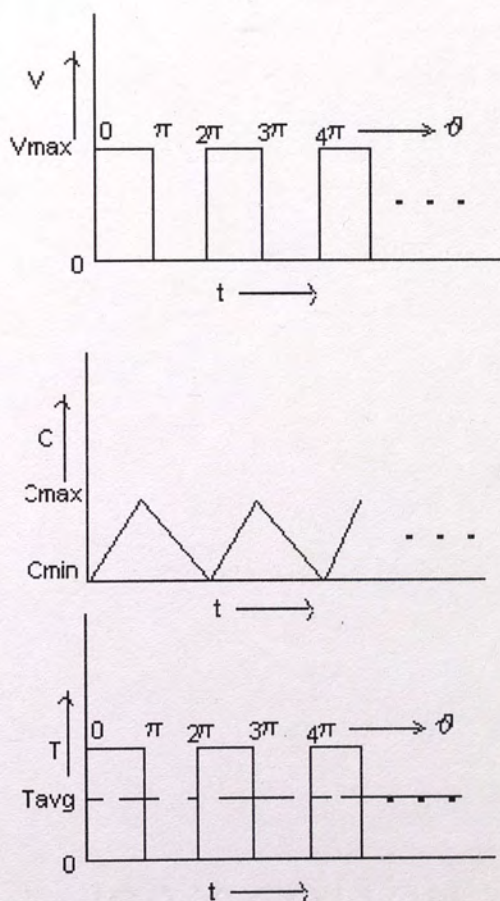


Figure 12 : Rectangular pulse, capacitance and torque waveforms.

Other voltage waveforms, such as sinusoidal alternating excitation, possibly rectified or superimposed on a d.c. voltage, are more readily available than a square-wave

voltage and may be more efficient for operating the rotor. fundamental frequency [29]. The design of the shapes of the electrodes is complicated by the fact that to maintain synchronism, the evolved capacitance variation is as nearly sinusoidal as possible for increasing efficiency. Also the nature of CMOS control circuits suggests that, digital pulse waveform is preferable to sinusoidal excitation owing to associated process simplicity.

At this point, it will be relevant to point out why axial drive motor actuation is chosen over side-drive one, where the rotor pole faces are adjacent to the edges of the stator pads. For a rotational displacement of the rotor pole by some angle θ relative to the stator pole face, the work involved in this displacement is equal to the change in initial stored energy U given by [30],

$$\Delta W = \Delta U = \frac{1}{2} V^2 \Delta C \quad (4.6)$$

Whereas, the displacement torque, T , for a tangential force, F on the rotor surface and pole arm length(roughly equals to rotor outer radius), l is given by,

$$\Delta W = Fl\Delta\theta = T\Delta\theta \quad (4.7)$$

Hence, capacitance variation and torque is related by,

$$T\Delta\theta = \frac{1}{2} V^2 \Delta C \quad (4.8)$$

The instantaneous start up torque depends on initial rotor position and is given by,

$$T(\theta) = \lim_{\Delta\theta \rightarrow 0} \frac{1}{2} V^2 \frac{\Delta C}{\Delta\theta} = \frac{1}{2} V^2 \frac{dC(\theta)}{d\theta} \quad (4.9)$$

The above is the equation for drive torque that is exerted for different rotor position variation. The term $dC(\theta)/d\theta$ can be chosen to provide orders of magnitude variation to generate the torque. For the side drive rotor, the varying overlap area is small, since this is determined by pole edge dimensions. On the other hand, for axial drive rotor, large variation in overlap area can be obtained by comparably large annular region present between outer and inner circular shape of both stator and rotor. To the designer's aid, additional drive on torque magnitude can be obtained by keeping the inner hollow circular disk diameter as small as possible and vice versa for the outer disk diameter, which essentially gives maximum capacitance modulation.

The other structural advancement that is present in the axial drive rotor-stator is the absence of bushing, which leads to considerable frictional wear for side-drive motor performance. The requirements of central hub and bushing structure cannot be eliminated from the design of side-drive motor, since stator and rotor pads have to be separately positioned and micromachined on the silicon wafer. This is contrasted by the axial drive configuration, where the rotor can be spatially levitated in the micron-sized separation space between stator and rotor which removes the frictional losses and wear and tear of the rotor surface while in continued rotation.

CHAPTER 5

A NUMERICAL ANALYSIS OF CRITICAL STRUCTURAL PARAMETERS OF THE ACTUATION UNIT FOR OPTIMIZED POWER OUTPUT

It has been reasoned out in the earlier section that for optimum power output and drive torque, variable-capacitance actuation is one viable option. The reason why VCM cannot be singled out as the only most power-efficient actuation method, will be explained in the following chapter in terms of equally viable asynchronous drive using charge relaxation method. But, the numerical investigation on the structural parameters involving stator and rotor-compressor assembly is focused on the variable-capacitance motor only in pursuit of an optimum design. The essential features to be considered are the capacitance variation with rotor position, the minimum rotor-stator separation without surmounting the breakdown field in the dielectric formed by liquid refrigerant R-134a and maximum excitation voltage level compatible with on-chip CMOS circuitry maximum drive level and obviously the waveforms shape, i.e., duty-cycle of the square pulse, type of pulse (unipolar or bipolar) or any other alternate waveform (sinusoidal, triangular), etc. For our calculation, it is assumed that the square wave pulse is generated on the stator pads, constituted by wedge-shaped electrodes. The choice of square wave

pulse is decided upon its digital nature and hence a on-chip CMOS logic circuit will be able to generate a three-phase pulse array. Since, it has been shown earlier that maximum capacitance variation is preferred for large tangential force or drive-torque to keep rotor in its highest rpm and trajectory, the shape and relative size of the pads, for example, electrode width, will determine high-area overlap charge distribution. Again the number and size of the pads are governed by electrode pitch length, i.e., minimum distance between adjacent pads constrained by λ or minimum feature length for successful mask definition. One of the significant advantage of miniaturization is the all forms of losses that are relevant in traditional machine-drive becomes negligible for small scale. Although certain reliability tolerance indispensable for VCM performance, may result in some losses, but for clarity and simplicity, they will be ignored. The relative significance of the major parameters, affecting the rotor-compressor performance and hence the maximum c.o.p. of the refrigerator, will be also discussed.

5.1 THEORETICAL CALCULATION OF TORQUE AND POWER

The previous simple schematic Figure 11 shows the edge view of a section of axially positioned stator-rotor assembly. The stator is underneath the rotor and has a number of planar wedge-shaped thin film pads or electrodes on its surface. The rotor will have a number almost equal to the number of stator pads, chosen to facilitate the starting torque to attain the synchronous speed in a minimum time lag. The electrical output of the on-chip CMOS drive circuitry is routed to the stator pads in a three-phase excitation mode to achieve the synchronous speed. In a synchronous electrostatic motor the capacitance C of the capacitor, formed by rotor-stator electrode overlap, is a function of

the angle of rotation, θ of the rotor. Now, a square wave pulse of voltage level V is applied to stator pads and varies periodically with time. When the motor is in rotation, θ is function of time and hence C is also. Electrical power is then converted into mechanical power determining compressor's performance. This power is calculated as follows [29].

If I is the current generated by on-chip CMOS voltage converter circuitry and supplied through the terminals to stator pads for a particular phase, then the transient electrical energy supplied in a time interval dt is given by:

$$P_e dt = IVdt \quad (5.1)$$

The varying charge on the electrodes is CV , and the change of is charge for the infinitesimal time interval is:

$$Idt = d(CV) = Cdv + VdC \quad (5.2)$$

From Eq. (5.1) and (5.2) we get,

$$P_e dt = CVdV + V^2 dC \quad (5.3)$$

Part of this energy is stored in the electrical field. The instantaneous field energy W_e is $1/2 CV^2$, and this increases in the time dt by an amount

$$dW_e = CVdV + \frac{1}{2} V^2 dC \quad (5.4)$$

The rest of the energy supplied is delivered to the rotor as mechanical energy $P_m dt$. The mechanical power is thus:

$$P_m = \frac{1}{2} V^2 dC / dt \quad (5.5)$$

The electro-mechanical torque T acting on the rotor is:

$$T = P_m dt / d\theta = \frac{1}{2} V^2 dC / d\theta \quad (5.6)$$

Therefore, the compressor's output power, which is essentially the mechanical power of rotor,

$$P_m = \omega_m T \quad (5.7)$$

where, $\omega_m = d\theta/dt$, is the angular velocity for the specified rpm of the rotor.

The waveform of varying spatio-temporal capacitance can be defined now. Supposing the number of electrodes to be M , the angle between two adjacent electrodes, the electrode pitch is then $2\pi/M$. The rotor position can be expressed in terms of an angular displacement parameter, Θ , with $\Theta = M\theta$; the parameter Θ varies by 2π when the rotor advances by one electrode. The capacitance, consequently, is a periodic function of Θ with a period 2π . When the rotor rotates uniformly and moves by one electrode in one period of supply voltage, this special case is attributed to 'synchronous' condition. The synchronous angular velocity ω_m equals ω_s/M , where ω_s is the angular frequency of the supply voltage. C is then seen to be periodic with supply voltage. From (5.5) and (5.6) it can be seen directly when a positive power and torque can be obtained. This occurs, for instance, if we have a rectangular voltage with $V \neq 0$ in that part of the period in which dC/dt is positive, and $V=0$ where dC/dt is negative. For best kinematical torque, the capacitance waveform should be triangular as shown earlier in Figure 12.

In general the rotor will lag in phase behind the voltage. The rotor position as also characterized previously by the parameter Θ , is given by:

$$\Theta = \omega_{sst} - \alpha \quad (5.8)$$

For part of the cycle the torque and power become negative and the average power and torque is smaller. The angle α is determined by a value such that the average torque balances out the torque required by the load. If the required torque is greater than the maximum torque of the rotor, the rotor falls out of synchronism and stops. In the case of a square-wave voltage, the pulse duty-cycle is a critical parameter in determining the maximum average power attainable out of rotor-integrated compressor's motion. From the Figure showing voltage and capacitance waveforms, respectively, if the length of cycle for which the pulse is present, i.e. $V^2 \neq 0$, and the triangular pulse duration for which $dC/dt > 0$ are of equal length, then the average power is maximum when the respective parts coincide. This means C_{min} coincides with the beginning of the square wave and C_{max} with the end point at which the pulse is switched off. The maximum average power in this case can be calculated by integrating Eq. (5.5) over a period as follows:

$$\overline{P}_{\max} = \frac{\int_0^T \frac{1}{2} V^2 \frac{dC}{dt} dt}{\int_0^T dt} \quad (5.9)$$

Since for the interval $(0, T/2)$, voltage is V_o and the capacitance varies linearly as a function of time and finally noting that $\omega_s T = 2\pi$, we get

$$\bar{P}_{\max} = \frac{1}{2} V_o^2 (C_{\max} - C_{\min}) \frac{\omega_s}{2\pi} \quad (5.10)$$

The maximum average torque follows from equation (5.7) as,

$$\bar{T}_{\max} = (M / 4\pi) V_o^2 (C_{\max} - C_{\min}) \quad (5.11)$$

A handful of remarks can be made based on the equations (5.10) and (5.11).

(1) P and T are proportional to V^2 . This implies that the sign of the voltage is irrelevant. To the rotor the voltage is equivalent to shown in Figure 12 earlier. With this nature of voltage, the rotor can be run synchronously without any inhibition.

(2) Given the magnitude of V_o , the frequency f_s of the square wave voltage (which can be determined from rotor's rpm) and the capacitance difference ($C_{\max} - C_{\min}$), the maximum average power \bar{P}_{\max} is independent of the number of electrodes M . In practice, there is a upper limit to M . If we start distributing more and more electrodes over a given rotor surface area, $C_{\max} - C_{\min}$ will gradually decrease and the expected increase to torque will not be attained. This is illustrated in Figure 12, depicted earlier.

(3) Design details of the stator and rotor assembly, such as gap width and electrode shapes, etc. are not explicitly contained in the above equations but is accounted for in the term ($C_{\max} - C_{\min}$). It is sufficient thus to measure the capacitance as a function of the position of the rotor without knowing much about structural pros and cons. The capacitance of an annular ring, as configured by the pancake rotor shape, can be formulated easily. Under the assumption that the minimum phase capacitance is much smaller than the maximum phase capacitance, the equation (5.11) simplifies to,

$$\overline{T}_{\max} = (M / 4\pi)V_o^2 C_{\max} \quad (5.12)$$

From the universal definition of capacitance between parallel faces of the poles, given by

$$C = \epsilon_o \epsilon_r \frac{A}{d} \quad (5.13)$$

where A is the area given by wl , w and l being the electrode width and length, and d is the separation between stator and rotor. If the number of phases in which the electrodes are arranged is denoted by n , R_o and R_i are the outer and inner radius of the stator and rotor disk, respectively and it is assumed that half of the annular ring is covered with pole faces, giving optimum capacitance variation, then the area is given by

$$A = \pi(R_o^2 - R_i^2) \frac{1}{2} \frac{1}{n} \quad (5.14)$$

With a three phase actuation, $n = 3$ and the overall capacitance based on equation (5.14) is given by,

$$C = \epsilon_r \epsilon_o \pi \frac{(R_o^2 - R_i^2)}{6d} \quad (5.15)$$

By combining equation (5.12) and (5.15), we get

$$\overline{T}_{\max} = (M / 4\pi)V_o^2 \epsilon_r \epsilon_o \pi \frac{(R_o^2 - R_i^2)}{6d} \quad (5.16)$$

Having formulated the fundamental set of equations that determine motor performance in axial-drive configuration, the next section discusses the design

requirements of the critical parameter for optimum power output of the compressor's rotor for a high c.o.p., which is a figure-of-merit for the performance of the proposed refrigerator.

5.2 OPTIMIZATION OF PARAMETERS FOR OPTIMUM POWER OUTPUT OF ROTOR-COMPRESSOR ACTUATION UNIT

For the prototype of the miniature mesoscopic refrigerator that will be implemented in silicon wafers, the design requirements are envisioned as follows:

1. Evaporating liquid temperature $T_{\text{evap}} = 12 \text{ }^{\circ}\text{C}$
2. Condensing vapor temperature $T_{\text{cond}} = 60 \text{ }^{\circ}\text{C}$.
3. Working fluid F 134a (1,1,1,2-tetrafluoroethane).

The compressor's output power level is a critical factor for the optimum compression ratio and high c.o.p. Based on the operating refrigerant's thermodynamic properties, a detailed thermodynamic feasibility analysis is performed, which can be viewed in Appendix A. For present focus of interest, the values of c.o.p. and compression ratio calculated for this refrigerant are listed below:

Coefficient of performance (c.o.p.) = 3.28 (large)

Compression ratio = 3.7 (large)

If the output power of the compressor is also sizeable to maintain the performance of the refrigerator in terms of the above parameters, the actuation module will also be yield-efficient with less area-integration and hence manufacturing package cost will be low. But the output power cannot be increased indefinitely and hence a parametric analysis of structural elements is required to come at a meaningful yet feasible solution. From the

design perspective, it means there will be compromise between the package area of such a manufacturable device and its deliverable power to the cooling load or circulating medium. It has been found that with adjustments with refrigerant's mass flow rate, the power the compressor can actually deliver, can be closely generated by the optimized mechanical power level of the compressor's rotor. A suitable value of the output power with all other structural parameters optimized, is outlined below:

The compressor's design guideline in meso-scale leads to following extracted values which are compatible with planar micromachining fabrication process:

4. Stator/rotor's disc's outer diameter, $D_o = 12 \text{ mm}$.
5. Stator/rotor's inner circular ring diameter, $D_i = 2 \text{ mm}$.
6. Compressor's rotating speed, $N = 439490 \text{ rpm}$

The above rotating speed is determined from vapor velocity at the tip of the compressor's vanes and is a function of the amount of work done for the compression performed. For the chosen refrigerant operating between the two temperature levels, the amount of work done on the refrigerant in providing the compression is fixed and hence the compressor's rpm is also a fixed parameter. The remaining are the core performance parameters, which require optimization.

7. Total number of rotor electrodes, $M = 450$.
8. The voltage pulse applied on the stator pads, $V_o = 250 \text{ volt}$
9. The rotor-stator separation, $d = 4 \times 10^{-6} \text{ m}$.
11. The permittivity of free space or air is, $\epsilon_o = 8.854 \times 10^{-12} \text{ farad/m}$.

All of the parameters from above deserve special attention. First, the voltage pulse value is shown to be related to maximum capacitance value obtainable and hence the drive

torque and power output. Although, the high value as warranted by output power level of the compressor is undesirable, the current state-of-the art power MOSFET switching circuits have already shown potential to attain such values for a particular range of frequencies. When the drive pulses have faster rise and fall time and shorter time period, it remains to be seen how the CMOS circuitry can attain the voltage level without faults or performance degradation. But the maximum value that can be applied to the stator pads is also conditioned by the breakdown field limit for the refrigerant in the separation space between rotor and underlying stator. Hence as the excitation voltage is increased and rotor-stator separation is decreased for higher torque and output power, the electrostatic field in the gap between the stator and the rotor rises sharply and reaches the breakdown limit. For the chosen values of voltage and separation gap, the maximum electrostatic field between rotor and stator is,

$$\frac{V_o}{d} = \frac{250}{4 \times 10^{-6}} \frac{V}{m} = 0.625 \times 10^8 V.m^{-1}$$

This value is below the breakdown magnitude level predicted for gap separations of the order of $1\mu m$ and certainly is not detrimental to device performance. Lastly, the value of relative permittivity of the liquid refrigerant has been referred as, $\epsilon = 2.6$ as per Freon.

With the above design parametric lists and equations for torque and power as shown in the previous section, the following derivation shows the optimum value of all the required parameters:

By putting the assigned values of respective parameters contained in equation (5.16), we get

The driving torque, $\tau_{avg} = 2.36 \times 10^{-4}$ newton-m

Assuming negligible rotor's ohmic loss and viscous drag and eliminating frictional loss on account of levitation mechanism yielding rotor suspended from stator in the gap, the maximum mechanical power output from compressor's rotor is,

$$P_{out} = \tau_{final} \times \omega_m \quad (5.17)$$

The rotational frequency of the compressor, also termed as mechanical frequency to differentiate from the excitation voltage-pulse frequency, is expressed in terms of compressor rpm.

$$\omega_m = \frac{2\pi N \text{ rad}}{60 \text{ sec}} = 4.602 \times 10^4 \frac{\text{rad}}{\text{sec}} \quad (5.18)$$

Finally, from equation (5.17), the extracted value of mechanical power output is,

$$P_{max} = 10.864 \text{ watt.}$$

The above value for output power will be enough for the intended compression ratio optimization. There remains one significant consideration as to the widths of the rotor and stator electrodes with respect to the chosen electrode number and maximum capacitance variation level. Obviously the electrode pitch needs to be much larger than the gap between stator and rotor for the expected large variation in capacitance. In addition, the minimum distance between adjacent layers needs to be compatible with the minimum feature length of fabrication, λ . A reasonable estimate of electrode width and the spacing width between adjacent electrodes can be calculated as follows:

Since, the pads are distributed in the area constrained by outer disc area and the inner hole area, the area of the annular ring between the two area is given by,

$$Area = \frac{\pi}{4} \times \{(12 \times 10^{-3})^2 - (2 \times 10^{-3})^2\} = 1.099 \times 10^{-4} m^2$$

The area of the wedge-shaped electrode can be closely approximated by,

$$area' = \frac{1}{2} M(R_o - R_i)^2 \sin \theta \quad (5.19)$$

By substituting the values and considering an 60% overlap of the whole area by the electrode area, the value of electrode width can be estimated.

$$\sin \theta = \frac{0.7 \times 1.099 \cdot 10^{-4}}{0.5 \times 100 / 4 \times 10^{-6} \times 450} rad = 0.0136 rad$$

Then, electrode width is $= (12 - 2) / 2 \times 10^{-3} \times 0.0136 = 68 \times 10^{-6} m$.

The spacing between adjacent electrodes can be calculated from the remaining area by following the above procedure.

The spacing width $= (R_o - R_i) \times \sin \theta = 5 \times 10^{-3} \cdot 5.86 \times 10^{-3} = 29.3 \times 10^{-6} m$.

In this configuration of rotor electrodes on the salient disc surface, the spacing width is much larger than the chosen gap width between stator and rotor. The relatively large value for both electrode and spacing widths respectively, indicates that mesoscale nature of the device configuration eliminates any doubt over compromising with minimum feature length, λ . Therefore, even with these large numbers of stator and rotor pads, the reproducibility and yield will be substantial with the current state-of-the art fabrication process. The extracted values of structural parameters are given below in Table 1.

Table 1

Critical structural parameters	Optimized Value
1. Outer diameter of rotor/stator disc	12×10^{-3} m.
2. Stator/rotor's inner central hub diameter	2×10^{-3} m.
3. The gap width between stator and rotor	4×10^{-6} m.
4. Number of stator phases	3
5. Total number of rotor pads (per phase)	150
6. The stator's excitation voltage	250 volt
7. Maximum capacitance (3 phase)	1.055×10^{-10} farad
8. Maximum drive torque	2.36×10^{-4} newton-m.
9. Maximum output power (3 phase)	10.86 watt

CHAPTER 6

AN OVERVIEW OF ELECTRO-QUASISTATIC INDUCTION MOTOR AND PERFORMANCE TRADE-OFF

Due to its structural simplicity and ease of design, the variable-capacitance miniature motor (VCM) has received most attention to date. Apart from the in-depth understanding of actuation principles, the stator drive voltage pulses are inherently simple and driving electronics are digital and interference-free, enabling the response time to be fast. However, several shortcomings of VCM performance have led to alternative motor structures to be taken into consideration. The inherent drawbacks that have acted as deterrents for widespread adoption of VCM for high-performance actuators are treated here sequentially.

First, in order to obtain the variable stator-rotor-overlap capacitance necessary for its operation, the rotor pads must be physically salient. Planarization over this saliency may require aggressive and exotic fabrication sequence. Second, in order to obtain large variation in capacitance and improved motor drive torque, the stator-rotor gap must be of the order of a few microns. This can pose fabrication difficulties in terms of rotor pad deposition during lithography. Also the relatively high rotor disk diameter to rotor-stator

separation ratio generates stability problem during rotation. Accidental sticking at the edges between stator and rotor is one of a number of phenomena, which adversely affect the device performance as the gap is shrunk to obtain high torque and motor rpm simultaneously. Thirdly, the synchronous operation has engendered concern about precise monitoring of rotor position during start up and while in rotation. The researchers also argue that VCM suffers from undesirable transverse force of electric origin that acts on the rotor and lead to wear and bushing friction. The last problem can be altogether counterbalanced by highly promising electrical levitation principle, which allows extra circuitry to enable rotor suspended in equilibrium in the micrometer gap between stator and rotor. Even if the continued innovations may be able to remove most of the drawbacks, the fabrication concerns of high-number of rotor pads definition during lithography steps seem to have propelled the MEMS researchers to pursue alternative drive principles such as rotary pancake electroquasistatic motor structures (IM) and piezoelectric motors. With regard to mesoscopic scale of interest, piezoelectric motors will not be able to generate the required high torque and rpm, since the piezoelectric drive are best suited to precision movements which are short-range in order. Also the high abundance of research study evident in literatures warrants that IM rotary-drive motor can provide the significant performance improvements over the variable capacitance motor in certain applications where a trade-off between VCM fabrication complexity and IM performance exists [31].

The key to induction drive over VCM is that IM is asynchronous in origin, thereby it produces steady-state motive torque at all velocities except the synchronous velocity. This drive feature acts as a favorable alternative to VCM's requirement of position-

control feedback. Secondly, the fabrication complexity constituted by rotor-pad deposition in VCM is absent in IM, since the pancake rotor can be constructed by a thin uniform layer of polysilicon or other material of suitable low conductivity which optimizes the motive torque at a given rotor rpm. This very fact reduces the required total mask steps in the fabrication process sequence. The next section details the performance dependencies of electro-quasistatic IM with respect to its structural elements.

6.1 INDUCTION MOTOR DRIVE PRINCIPLE AND PERFORMANCE-CRITICAL PARAMETERS

In the previous chapter, the performance of variable capacitance motor is analyzed with respect to specified structural parameters. Although the principal focus of the current study is on VCM performance for optimized output power at a given rpm of rotor, IM performance by itself generates topics of alternate research study, which has been essentially undertaken for an overall realization and comparative performance trade-off contrasted by VCM. Therefore, this chapter is designed to enlighten the general operational principles and performance dependency study and more thorough analysis is reserved for future work.

The structural difference between IM and VCM is that in the case of IM, the rotor is an annular disk with a thin metal layer having uniform permittivity and conductivity. The rotational force exerted on the rotor is accomplished by azimuthally traveling sinusoidal waves of equal temporal and spatial frequency on the stator pads. As the potential waves travel on the sets of stator pads, they induce free electric charges of opposite charges on the rotor surface. These image charges propagate in synchronism with the potential

waves applied to the stator pad array, but, following charge relaxation in the rotor and stator-rotor gap, these charges lag behind. The resulting azimuthal displacement between the potential waves and the image charges gives rise to a motive torque acting on the rotor. If the dominant charge relaxation time is prolonged due to lower rpm of the rotor, very little image charges are induced. On the other hand, higher rotor velocity than synchronous operation leads to abrupt charge relaxation time resulting in the image charges' being slightly displaced from the potential waves. Both conditions reduce motive torque. It has been proven and depicted in a model by the authors [31] that there exists an optimal set of IM material properties for a given IM geometry and excitation and hence the structural parametric dependency is more intensive and complex with regard to optimal IM performance.

The motive torque, which is a central design parameter, is a function of the rotor film conductivity. As the motive torque and transverse force change with varying conductivity of the rotor film, so too does the torque balance that establishes the steady-state rotor speed. The authors of the cited paper [31] have demonstrated this feature in their analysis and found the optimum rotor velocity for maximum motive torque at a rotor conductivity of 10^{-4} S(siemens) which is the limiting conductivity of an undoped silicon. However, as the rotor rpm is required to attain the sizeable value as optimized in the case of VCM in the previous analysis, low conductivity values are desired and this imposes strenuous control of dopants in polysilicon deposition process. Consequently, it suffices to say that although the fabrication advantage may prompt the designer to adopt IM actuation, it may be difficult to reliably fabricate an IM with a pre-specified performance that is feasible with variable capacitance motor. Alternate materials, which are

conformable to thin film deposition processes on silicon and simultaneously provide lower conductivity, are pursued of late for a solution. The next set of design parameter deserving attention is IM axial dimensions. In general, their dependence over a wide range of operating conditions is quite complex. As the axial gap between stator and rotor is increased to tens of microns, the transverse rotor force decreases as a square of the axial gap dimension, so that the rotor surface and edge wear can be significantly reduced. The axial gap control also leads to ease of lithographic fabrication during masking steps. The third set of design parameter is rotor-velocity-dependent charge-relaxation time. Depending on the lower or faster velocity of the rotor, opposite and like nature image charges are induced on the rotor film. Therefore three velocities can be detected at which the motive torque, frictional load torque and windage load torque balance at steady state, respectively. In short, an inherent stabilizing effect on the rotor can be set up by the control of charge relaxation time.

Obviously the large set of performance dependence stems from control circuitry. Although the drive circuitry may be involved due to the varying potential amplitude requirement on the stator pads for spatial contingency, the rotor-feedback positional sensing circuitry, which would be required in VCM drive, acts a performance trade-off leading to compact IC feasibility for IM. On the negative side, even though the voltage on the stator pads is assumed to be represented by a sinusoidal wave, the minimum feature size of lithography dictates the maximum number of stator pads that can be fabricated. Hence at higher drive frequencies, variation along the stator of the rotating electromagnetic field distorts the actual three phase voltage shape far from ideal. This leads to generation of higher order harmonics which interact to the motive torque which

are not accounted for in the calculation. Nor is it immediately clear what amplitude should be assigned to the sinusoidal voltage in the theoretical calculation so that it closely resembles the real one. The designer's task is therefore intensely complicated with respect to IM performance optimization, which takes care of structural dependencies with that of design specifications. The design margin and tolerance offered by variable capacitance motor is simpler and should not be overlooked in the case of comparable performance.

CHAPTER 7

CONCLUSION AND FUTURE WORK

The orders of economies in regard to mass-reproducibility of miniaturized systems have shown tremendous market potential in energy-efficient applications of micro and meso-technology based systems. In addition, the researchers have co-echoed the views that the next generation of microactuator will be designed to have sheet architectural integration to provide high work-to-work conversion in heat-pump and engine-based energy-transduction applications which will provide lower capital cost per wafer than their macro alternative. The different hierarchical module integration to realize a complete functional system such as air-conditioner, refrigerator, heat engine, etc., is gradually pushing the MEMS domain to be drafted into meso-scale domain, which constitutes the overall system as dimensions of millimeter. As a result, more drive power and energy output can be extracted as harvests from this inevitable migration, which also makes the durability of the entire system to be robust for their comparably large size with respect to MEMS. The feasibility of “turbine on a dime”- as a number of researchers put forth in a recent article [3], aids as a support to this observation.

The aim of this thesis work is directed to thermodynamic performance analysis of such mesoscopically miniaturized refrigerator within a few centimeters of packaging

dimensions. The basic structural module design into a highly-efficient working system has been explored with reference to certain prototypes. The design prototypes will assist in realization of the module from a process fabrication standpoint. Also, after identifying the key motor-compressor actuation unit, which ultimately determines the refrigerator's performance in terms of c.o.p. and extractable power, the structural configurations are outscored for performance trade-off. The variable capacitance axial-drive motor performance has shown promise to obtain the design-specified power value within a few margins and a numerical parametric analysis is made in support of this finding. An increasing amount of interest is also seen to be devoted to induction motor drive for their inherent fabrication simplicity. In-depth analysis of such IM performance is currently under intense study and reaching completion. This thesis work formulates the key concepts behind performance optimization of the entire refrigerator's reliable operation. The further work is devoted to computer-aided module design and mask manufacturing to ultimately fabricate individual parts. Next, a number of silicon-to-silicon die bonding will be necessary to build the overall refrigerator system with its cohesive building modules.

Some of the major challenges posed for such multilevel module-integrated refrigerator design are addressed at this point. The electrical levitation of revolving rotor in the thin gap between underlying stator for rotor stability has generated growing optimism as well as debatable issues. The electrical levitation is crucial in VCM performance, since the gap between stator and rotor cannot be enlarged from a few microns to effect higher drive torque and power. As a result of this, the relatively large rotor-compressor weight might generate accidental sticking on the stator when the rotor edge wobbles with respect to stator, regardless the levitation circuitry whose balancing or

stabilizing force may not be strong enough to sustain this mass loading. Therefore, the structural orientations of rotor and stator needs to be adjusted so that the working fluid can be conveniently flowed to provide significant balancing thrust to hold the rotor-compressor in levitation from stator. As one of the prime issue, the on-chip circuit architecture must have provisions for the levitation and control circuitry apart from establishing digitized or three-phase excitation of stator pads and maintaining synchronization of the pulses to provide maximum overlapping capacitance. In addition to this, temperature-sensing circuitry has to be co-fabricated in IC as a part of the overall circuitry. All of the above requirements generate significant IC area overhead and layout-driven analysis may be necessary to incorporate such circuitry in perfect agreement to entire motor-compressor unit design guidelines.

The other retarding considerations emanate from the stringent temperature control of evaporator plate (12°C) and condenser plate (60°C), respectively, while the working fluid is in flow between the chambers. The heat-insulating thin films can be layered onto the silicon surface to combat this temperature migration, but the nature and selection of such films is a topic of further research. Lastly, the microlithographic routing of the contact metalization to the stator pads with respect to IC signal generator remains an issue. The contiguous pads on the stator, receiving different phase voltage magnitude or polarity of digitized pulses, have to be electrically isolated from each other so that the different voltage levels do not get merged and corrupt the device performance. This necessitates multilevel dielectric isolation layers between the thin film pads, arranged in a three phase sequential assembly and results in complex masking design and process integration.

The growing abundance of research innovations to combat each of the cited challenges suggests that the designers will ultimately be able to realize vast superior performance in near future from such energy devices.

Appendix A

Kinematical performance analysis of variable capacitance motor

Analysis of design requirements of mm-scale variable capacitance rotary disk motor

The optimal design parameters required are :

Outer electrode diameter, $D_o = 12 \text{ .mm}$

Inner electrode diameter, $D_i = 2 \text{ .mm}$

Compressor rotating speed, $N = 439490 \text{ rpm}$

Outer electrode radius, $R_o = D_o/2 \text{ .mm}$

Inner electrode radius, $R_i = D_i/2 \text{ .mm}$

Compressor's angular speed :

$$\omega := \frac{2 \cdot \pi \cdot N \text{ rad}}{60 \text{ sec}} \quad \omega = 4.602 \cdot 10^4 \cdot \text{sec}^{-1}$$

For a design goal of electromechanical power output in the vicinity of 11 watt, the following parameters are configured to fit the optimal design set up:

Number of stator pads(per phase), $M = 150$

Disk rotor thickness , $T = 200 \cdot 10^{-6} \text{ .m}$

Rotor-stator separation, $d = 4 \times 10^{-6} \text{ .m}$

Maximum excitation voltage $V_o = 250 \text{ V.}$

The mass-density of silicon, $\rho_r = 2.33 \times 10^3 \text{ kg-m}^3$

The analysis will be provided from rotor kinematics:

The electrical torque τ_e produced by a variable capacitance motor is determined by the spatial rate of change of its stored electric energy .

Using W_e as stored electric coenergy ,

$$\tau_e = d W_e / d \theta \quad \dots\dots\dots (1)$$

The stored electrical energy for each phase is,

$$W_{ep} = 1/2 C_p(\theta) \cdot V_p^2$$

Then for each phase torque becomes :

$$\tau_{ep} = 1/2 \cdot V_p^2 \cdot d C_p(\theta) / d \theta \quad \dots\dots\dots (2)$$

For the present purposes , only the average electric torque is needed to be extracted. Thus , the torques of the individual phases are time averaged and summed to yield an total average torque. For each phase , the excitation voltage is assumed to be constant at V_0 when the capacitance is increasing and zero otherwise .This is the synchronous excitation required for maximum torque production.

For a planar rotary disk configuration ,

$$(C_p(\theta))_{max} = \epsilon \cdot (R_o^2 - R_i^2) / (6 \cdot d) \quad \dots\dots\dots (3)$$

$$\epsilon_r = 2.6 \quad \text{Assumed for R-134}$$

$$\epsilon_o = 8.854 \cdot 10^{-12} \cdot \text{farad} \cdot \text{m}^{-1}$$

$$\epsilon = \epsilon_o \cdot \epsilon_r \quad \epsilon = 2.302 \cdot 10^{-11} \cdot \text{farad} \cdot \text{m}^{-1}$$

But the actual maximum phase capacitance will also depend on the number and size of rotor and stator electrodes. The minimum feature size of the fabrication process λ defines the size of the space between adjacent electrodes and hence determines their maximum size.

$$C_{pmax} = \epsilon \cdot \frac{\pi \cdot (R_o^2 - R_i^2)}{6 \cdot d}$$

$$C_{pmax} = 1.055 \cdot 10^{-10} \text{ F.}$$

Using the capacitance waveform plotted in Figure 12 of the paper and the following relation:

$$P_{out} = 1/2 \cdot dC_p/dt \cdot V_p^2$$

Assuming negligible loss, the electromechanical power output can be calculated

$$P_{out} = \frac{1}{2} \cdot V_o^2 \cdot M \cdot \frac{\omega}{2 \cdot \pi} \cdot C_{pmax}$$

$$P_{out} = 3.621 \text{ watt}$$

$$\text{For three phase, } P_{max} = 3 \cdot P_{ou}$$

$$P_{max} = 10.864 \text{ W}$$

The maximum average overall torque is :

$$\tau_{avg} = \frac{P_{max}}{\omega} \quad \tau_{avg} = 2.36 \cdot 10^{-4} \text{ m} \cdot \text{newto}$$

The key design parameters:

Number of stator/rotor pads, $M = 150$ (per phase).

Rotor-stator separation, $d = 4 \mu\text{m}$

Maximum voltage induced on stator pads, $V_o = 250 \text{ V}$.

The other required design parameters have been clustered in Table 1.

LIST OF REFERENCES

- [1] W. N. Trimmer, "Micromechanics and MEMS : Classic and Seminal Papers to 1990", IEEE Order No. PC 4390, pp. 117-139, 1997.
- [2] W. N. Trimmer, "Microrobots and Micromechanical Systems", Sensors & Actuators, Vol. 19, No. 3, pp. 267-287, September 1989.
- [3] R. S. Wegeng and M. K. Drost, "Developing New Miniature Energy Systems", Mechanical Engineering, pp. 82-85, September 1994.
- [4] Jennifer Porro, "Mighty Microrobots: Berkeley Research Highlights", Berkeley Engineering, pp. 18-19, 1998.
- [5] <http://www.darpa.mil/eto/MEMS/2003/showslide.html>, 1999
- [6] Kaveh Azhar, "A thermal management epidemic in need of a cure", Electronics Cooling, Volume 5, Number 1, pp. 1-4, January 1999.
- [7] M. Sakata, Y. HataZawa, A. Omodaka, T. Kudoh et al., "An Electrostatic Top Motor and Its Characteristics", Transducers'89, Proceedings of the 5th International Conference on Solid-State Sensors and Actuators and Eurosensors III, Vol. 2, pp. 168-172, June 1990.
- [8] A. G. Frangoul and K. B. Sundaram, "Design and Fabrication Process for Electrostatic Side-drive Motors", Journal of Micromechanics and Microengineering, Vol.5, pp. 11-17, 1995.
- [9] X. Y. He, Y. Huang, Z.Y. Zhou et al., "A Magnetic Levitation Actuator for Micro-

- Assembly”, Transducers '97: 1997 International Conference on Solid-State Sensors and Actuators, pp. 797-799, 1997.
- [10] U. Beerschwinger et al., “Coupled Electrostatic and Mechanical FEA of a Micro-motor”, Journal of MicroElectroMechanical Systems, vol. 3, No.4, pp. 162-170, 1994.
- [11] Anita M. Flynn et al., “Piezoelectric Micromotors for Microrobots”, Journal of MicroElectroMechanical Systems, Vol. 1, No.1, pp. 44-51, March 1992.
- [12] F. C. M. Van De Pol, “A Thermo-Pneumatic Actuation Principle for a Micromini-ature Pump and other Micromechanical Devices”, Sensors and Actuators, Vol. 17, pp. 139-143, 1989.
- [13] P. Krulevitch et al., “Thin Film Shape Memory Alloy Microrobots”, Journal of Mi-croElectroMechanical Systems, Vol. 5, No.4, pp. 270-280, December 1996.
- [14] Thomas M. Flynn, “Refrigeration and Liquefaction”, Chapter 6, Cryogenic Engine-ering, Marcel Dekker Inc., pp. 273-277, 1997.
- [15] R. J. Dossart, “Refrigeration and The Vapor Compression System”, Chapter 6, Prin-ciples of Refrigeration, John Wiley and Sons, 2nd Ed., pp. 110-112, 1978.
- [16] Thomas M. Flynn, “Cryogenic Fluids”, Chapter 3, Cryogenic Engineering, Marcel Dekker Inc., pp. 71-180, 1997.
- [17] <http://www.rittal-corp.com/newsonline/july/breakingnews.html#micro>, 1999.
- [18] R. J. Dossart, “Cycle Diagrams and Simple Saturated Cycle”, Chapter 7, Principles of Refrigeration, John Wiley and Sons, 2nd Ed., pp. 123-141, 1978.
- [19] S. A. Jacobson, “Aerothermal Challenges in the Design of a Microfabricated Gas

Turbine Engine”, American Institute of Aeronautics and Astronautics, Inc., pp. 1-11, 1998.

[20] A. H. Epstein et al., “Micro-Heat Engines, Gas Turbines, and Rocket Engines- The MIT Microengine Project”, American Institute of Aeronautics and Astronautics, Inc., pp. 1-12, 1997.

[21] Y. C. Tai et al., “IC-Processed Micromotors: Design, Technology and Testing”, Proceedings IEEE MicroElectroMechanical Systems, pp. 1-6, February 1989.

[22] W. N. Carr et al., “On-Chip Integration of High Voltage Generator Circuits for an Electrostatic Micromotor”, Transducers '95: The 8th International Conference on Solid State Sensors and Actuators, pp. 150-153, 1995.

[23] N. I. Maluf et al., “High-Voltage Devices and Circuits Fabricated Using Foundry CMOS for Use With Electrostatic MEMS Actuators”, Transducers '95: The 8th International Conference on Solid State Sensors and Actuators, pp. 150-153, 1995.

[24] S. Kumar et al., “A Proposal for Electrically Levitating Micromotors”, Sensors & Actuators A, Vol. 24, pp. 141-149, 1990.

[25] G. H. He et al., “Electrical Levitation of Micromotors and Microaccelerometers”, Transducers '95: The 8th International Conference on Solid State Sensors & Actuators, pp. 442-445, 1995.

[26] <http://www.grc.nasa.gov/WWW/chemsensors>, 1996.

[27] A. Majumdar et al., “Micro Power Devices”, Microscale Thermophysical Engineering, 2nd Ed., pp. 67-69, 1998.

[28] W. S. N. Trimmer et al., “Design Considerations for a Practical Electrostatic Micromotors”, Sensors & Actuators, vol. 11, pp. 189-206, 1987.

- [29] B. Bolle'e, "Electrostatic Motors", Philips Technical Review, Vol. 30, pp. 178-194, 1969.
- [30] S. F. Bart et al., " Design Considerations for Micromachined Electric Actuators", Sensors & Actuators, Vol. 14, pp. 269-292, 1988.
- [31] S. F. Bart et al., "ElectroQuasistatic Induction Motors", Proceedings IEEE Micro-ElectroMechanical Systems, pp. 7-12, February 1989.